Observation of four-wave mixing in slow-light silicon photonic crystal waveguides

James F. McMillan,[1] Mingbin Yu,[2] Dim-Lee Kwong,[2] and Chee Wei Wong[1,*]

[1]*Optical Nanostructures Laboratory, Center for Integrated Science and Engineering, Solid-State Science and Engineering, and Mechanical Engineering, Columbia University, New York, NY 10027, USA*
[2]*Institute of Microelectronics, Singapore, 117685, Singapore*
**cww2104@columbia.edu*

Abstract: Four-wave mixing is observed in a silicon W1 photonic crystal waveguide. The dispersion dependence of the idler conversion efficiency is measured and shown to be enhanced at wavelengths exhibiting slow group velocities. A 12-dB increase in the conversion efficiency is observed. Concurrently, a decrease in the conversion bandwidth is observed due to the increase in group velocity dispersion in the slow-light regime. The experimentally observed conversion efficiencies agree with the numerically modeled results.

OCIS codes: (130.5296) Photonic crystal waveguides; (190.4380) Nonlinear optics, four-wave mixing

References and links

1. H. Fukuda, K. Yamada, T. Shoji, M. Takahashi, T. Tsuchizawa, T. Watanabe, J. Takahashi, and S. Itabashi, "Four-wave mixing in silicon wire waveguides," Opt. Express **13**(12), 4629–4637 (2005).
2. R. Espinola, J. Dadap, R. Osgood, Jr., S. McNab, and Y. Vlasov, "C-band wavelength conversion in silicon photonic wire waveguides," Opt. Express **13**(11), 4341–4349 (2005).
3. M. A. Foster, A. C. Turner, R. Salem, M. Lipson, and A. L. Gaeta, "Broad-band continuous-wave parametric wavelength conversion in silicon nanowaveguides," Opt. Express **15**(20), 12949–12958 (2007).
4. M. A. Foster, A. C. Turner, J. E. Sharping, B. S. Schmidt, M. Lipson, and A. L. Gaeta, "Broad-band optical parametric gain on a silicon photonic chip," Nature **441**(7096), 960–963 (2006).
5. A. C. Turner, M. A. Foster, A. L. Gaeta, and M. Lipson, "Ultra-low power parametric frequency conversion in a silicon microring resonator," Opt. Express **16**(7), 4881–4887 (2008).
6. M. Ferrera, L. Razzari, D. Duchesne, R. Morandotti, Z. Yang, M. Liscidini, J. E. Sipe, S. Chu, B. E. Little, and D. J. Moss, "Low-power continuous-wave nonlinear optics in doped silica glass integrated waveguide structures," Nat. Photonics **2**(12), 737–740 (2008).
7. C. Koos, P. Vorreau, T. Vallaitis, P. Dumon, W. Bogaerts, R. Baets, B. Esembeson, I. Biaggio, T. Michinobu, F. Diederich, W. Freude, and J. Leuthold, "All-optical high-speed signal processing with silicon–organic hybrid slot waveguides," Nat. Photonics **3**(4), 216–219 (2009).
8. M. R. Lamont, B. Luther-Davies, D. Y. Choi, S. Madden, X. Gai, and B. J. Eggleton, "Net-gain from a parametric amplifier on a chalcogenide optical chip," Opt. Express **16**(25), 20374–20381 (2008).
9. Y. H. Kuo, H. Rong, V. Sih, S. Xu, M. Paniccia, and O. Cohen, "Demonstration of wavelength conversion at 40 Gb/s data rate in silicon waveguides," Opt. Express **14**(24), 11721–11726 (2006).
10. B. G. Lee, A. Biberman, N. Ophir, A. C. Turner-Foster, M. A. Foster, M. Lipson, A. L. Gaeta, and K. Bergman, "160-Gb/s Broadband Wavelength Conversion on Chip Using Dispersion-Engineered Silicon Waveguides," in *CThBB1* (OSA, 2009).
11. R. Salem, M. A. Foster, A. C. Turner, D. F. Geraghty, M. Lipson, and A. L. Gaeta, "Signal regeneration using low-power four-wave mixing on silicon chip," Nat. Photonics **2**(1), 35–38 (2008).
12. O. Kuzucu, Y. Okawachi, R. Salem, M. A. Foster, A. C. Turner-Foster, M. Lipson, and A. L. Gaeta, "Spectral phase conjugation via temporal imaging," Opt. Express **17**(22), 20605–20614 (2009).
13. M. A. Foster, R. Salem, Y. Okawachi, A. C. Turner-Foster, M. Lipson, and A. L. Gaeta, "Ultrafast waveform compression using a time-domain telescope," Nat. Photonics **3**(10), 581–585 (2009).
14. R. Salem, M. A. Foster, A. C. Turner, D. F. Geraghty, M. Lipson, and A. L. Gaeta, "Optical time lens based on four-wave mixing on a silicon chip," Opt. Lett. **33**(10), 1047–1049 (2008).
15. R. Salem, M. A. Foster, A. C. Turner-Foster, D. F. Geraghty, M. Lipson, and A. L. Gaeta, "High-speed optical sampling using a silicon-chip temporal magnifier," Opt. Express **17**(6), 4324–4329 (2009).
16. Y. Okawachi, R. Salem, M. A. Foster, A. C. Turner-Foster, M. Lipson, and A. L. Gaeta, "High-resolution spectroscopy using a frequency magnifier," Opt. Express **17**(7), 5691–5697 (2009).

#126813 - $15.00 USD Received 12 Apr 2010; revised 22 Jun 2010; accepted 22 Jun 2010; published 7 Jul 2010

17. M. A. Foster, R. Salem, D. F. Geraghty, A. C. Turner-Foster, M. Lipson, and A. L. Gaeta, "Silicon-chip-based ultrafast optical oscilloscope," Nature **456**(7218), 81–84 (2008).
18. M. Notomi, K. Yamada, A. Shinya, J. Takahashi, C. Takahashi, and I. Yokohama, "Extremely large group-velocity dispersion of line-defect waveguides in photonic crystal slabs," Phys. Rev. Lett. **87**(25), 253902 (2001).
19. Y. A. Vlasov, M. O'Boyle, H. F. Hamann, and S. J. McNab, "Active control of slow light on a chip with photonic crystal waveguides," Nature **438**(7064), 65–69 (2005).
20. T. F. Krauss, "Slow light in photonic crystal waveguides," J. Phys. D Appl. Phys. **40**(9), 2666–2670 (2007).
21. T. Baba, "Slow light in photonic crystals," Nat. Photonics **2**(8), 465–473 (2008).
22. H. Oda, K. Inoue, A. Yamanaka, N. Ikeda, Y. Sugimoto, and K. Asakawa, "Light amplification by stimulated Raman scattering in AlGaAs-based photonic-crystal line-defect waveguides," Appl. Phys. Lett. **93**(5), 051114 (2008).
23. J. F. McMillan, M. Yu, D. Kwong, and C. W. Wong, "Observation of spontaneous Raman scattering in silicon slow-light photonic crystal waveguides," Appl. Phys. Lett. **93**(25), 251105 (2008).
24. C. Husko, S. Combrié, Q. V. Tran, F. Raineri, C. W. Wong, and A. De Rossi, "Non-trivial scaling of self-phase modulation and three-photon absorption in III-V photonic crystal waveguides," Opt. Express **17**(25), 22442–22451 (2009).
25. Y. Hamachi, S. Kubo, and T. Baba, "Slow light with low dispersion and nonlinear enhancement in a lattice-shifted photonic crystal waveguide," Opt. Lett. **34**(7), 1072–1074 (2009).
26. H. Oda, K. Inoue, Y. Tanaka, N. Ikeda, Y. Sugimoto, H. Ishikawa, and K. Asakawa, "Self-phase modulation in photonic-crystal-slab line-defect waveguides," Appl. Phys. Lett. **90**(23), 231102 (2007).
27. S. Combrié, Q. V. Tran, A. De Rossi, C. Husko, and P. Colman, "High quality GaInP nonlinear photonic crystals with minimized nonlinear absorption," Appl. Phys. Lett. **95**(22), 221108 (2009).
28. K. Inoue, H. Oda, N. Ikeda, and K. Asakawa, "Enhanced third-order nonlinear effects in slow-light photonic-crystal slab waveguides of line-defect," Opt. Express **17**(9), 7206–7216 (2009).
29. B. Corcoran, C. Monat, C. Grillet, D. J. Moss, B. J. Eggleton, T. P. White, L. O'Faolain, and T. F. Krauss, "Green light emission in silicon through slow-light enhanced third-harmonic generation in photonic-crystal waveguides," Nat. Photonics **3**(4), 206–210 (2009).
30. C. Monat, B. Corcoran, M. Ebnali-Heidari, C. Grillet, B. J. Eggleton, T. P. White, L. O'Faolain, and T. F. Krauss, "Slow light enhancement of nonlinear effects in silicon engineered photonic crystal waveguides," Opt. Express **17**(4), 2944–2953 (2009).
31. M. Ebnali-Heidari, C. Monat, C. Grillet, and M. K. Moravvej-Farshi, "A proposal for enhancing four-wave mixing in slow light engineered photonic crystal waveguides and its application to optical regeneration," Opt. Express **17**(20), 18340–18353 (2009).
32. Y. Liu, and C. Jiang, "Enhanced parametric amplification in slow-light photonic crystal waveguides," Chin. Sci. Bull. **54**(13), 2221–2224 (2009).
33. K. Masao, K. Eiichi, S. Akihiko, T. Takasumi, and N. Masaya, "Optical Kerr Nonlinearity in Silicon Photonic Crystal Waveguides-Four-Wave Mixing Process-," IEIC Technical Report (Institute of Electronics, Information and Communication Engineers) **106**, 55–58 (2006).
34. V. Eckhouse, I. Cestier, G. Eisenstein, S. Combrié, P. Colman, A. De Rossi, M. Santagiustina, C. G. Someda, and G. Vadalà, "Highly efficient four wave mixing in GaInP photonic crystal waveguides," Opt. Lett. **35**(9), 1440–1442 (2010).
35. K. Suzuki, Y. Hamachi, and T. Baba, "Fabrication and characterization of chalcogenide glass photonic crystal waveguides," Opt. Express **17**(25), 22393–22400 (2009).
36. M. Soljacić, and J. D. Joannopoulos, "Enhancement of nonlinear effects using photonic crystals," Nat. Mater. **3**(4), 211–219 (2004).
37. J. Hansryd, P. Andrekson, M. Westlund, J. Li, and P. Hedekvist, "Fiber-based optical parametric amplifiers and their applications," IEEE J. Sel. Top. Quantum Electron. **8**(3), 506–520 (2002).
38. M. Dinu, F. Quochi, and H. Garcia, "Third-order nonlinearities in silicon at telecom wavelengths," Appl. Phys. Lett. **82**(18), 2954 (2003).
39. J. F. McMillan, X. Yang, N. C. Panoiu, R. M. Osgood, and C. W. Wong, "Enhanced stimulated Raman scattering in slow-light photonic crystal waveguides," Opt. Lett. **31**(9), 1235–1237 (2006).
40. S. Assefa, and Y. A. Vlasov, "High-order dispersion in photonic crystal waveguides," Opt. Express **15**(26), 17562–17569 (2007).
41. S. Johnson, and J. Joannopoulos, "Block-iterative frequency-domain methods for Maxwell's equations in a planewave basis," Opt. Express **8**(3), 173–190 (2001).
42. M. Notomi, A. Shinya, S. Mitsugi, E. Kuramochi, and H. Ryu, "Waveguides, resonators and their coupled elements in photonic crystal slabs," Opt. Express **12**(8), 1551–1561 (2004).
43. E. Dulkeith, S. J. McNab, and Y. A. Vlasov, "Mapping the optical properties of slab-type two-dimensional photonic crystal waveguides," Phys. Rev. B **72**(11), 115102 (2005).
44. D. M. Beggs, L. O'Faolain, and T. F. Krauss, "Accurate determination of hole sizes in photonic crystal slabs using an optical measurement," Physica E **41**(6), 1115–1117 (2009).
45. M. Settle, M. Salib, A. Michaeli, and T. F. Krauss, "Low loss silicon on insulator photonic crystal waveguides made by 193nm optical lithography," Opt. Express **14**(6), 2440–2445 (2006).

#126813 - $15.00 USD Received 12 Apr 2010; revised 22 Jun 2010; accepted 22 Jun 2010; published 7 Jul 2010

46. L. Jia, M. Geng, L. Zhang, L. Yang, P. Chen, Y. Liu, Q. Fang, and M. Yu, "Effects of waveguide length and pump power on the efficiency of wavelength conversion in silicon nanowire waveguides," Opt. Lett. **34**(22), 3502–3504 (2009).
47. J. P. Hugonin, P. Lalanne, T. P. White, and T. F. Krauss, "Coupling into slow-mode photonic crystal waveguides," Opt. Lett. **32**(18), 2638–2640 (2007).
48. R. J. P. Engelen, D. Mori, T. Baba, and L. Kuipers, "Two regimes of slow-light losses revealed by adiabatic reduction of group velocity," Phys. Rev. Lett. **101**(10), 103901 (2008).
49. J. Li, T. P. White, L. O'Faolain, A. Gomez-Iglesias, and T. F. Krauss, "Systematic design of flat band slow light in photonic crystal waveguides," Opt. Express **16**(9), 6227–6232 (2008).
50. D. Mori, S. Kubo, H. Sasaki, and T. Baba, "Experimental demonstration of wideband dispersion-compensated slow light by a chirped photonic crystal directional coupler," Opt. Express **15**(9), 5264–5270 (2007).
51. E. Kuramochi, M. Notomi, S. Hughes, A. Shinya, T. Watanabe, and L. Ramunno, "Disorder-induced scattering loss of line-defect waveguides in photonic crystal slabs," Phys. Rev. B **72**(16), 161318 (2005).
52. S. Hughes, L. Ramunno, J. F. Young, and J. E. Sipe, "Extrinsic optical scattering loss in photonic crystal waveguides: role of fabrication disorder and photon group velocity," Phys. Rev. Lett. **94**(3), 033903 (2005).
53. L. O'Faolain, T. P. White, D. O'Brien, X. Yuan, M. D. Settle, and T. F. Krauss, "Dependence of extrinsic loss on group velocity in photonic crystal waveguides," Opt. Express **15**(20), 13129–13138 (2007).
54. N. Le Thomas, H. Zhang, J. Jágerská, V. Zabelin, R. Houdré, I. Sagnes, and A. Talneau, "Light transport regimes in slow light photonic crystal waveguides," Phys. Rev. B **80**(12), 125332 (2009).
55. F. Morichetti, A. Canciamilla, C. Ferrari, M. Torregiani, A. Melloni, and M. Martinelli, "Roughness induced backscattering in optical silicon waveguides," Phys. Rev. Lett. **104**(3), 033902 (2010).
56. M. Patterson, S. Hughes, S. Combrié, N. V. Tran, A. De Rossi, R. Gabet, and Y. Jaouën, "Disorder-induced coherent scattering in slow-light photonic crystal waveguides," Phys. Rev. Lett. **102**(25), 253903 (2009).
57. M. Patterson, S. Hughes, S. Schulz, D. M. Beggs, T. P. White, L. O'Faolain, and T. F. Krauss, "Disorder-induced incoherent scattering losses in photonic crystal waveguides: Bloch mode reshaping, multiple scattering, and breakdown of the Beer-Lambert law," Phys. Rev. B **80**(19), 195305 (2009).
58. G. Agrawal, *Nonlinear Fiber Optics*, 3rd ed. (Academic Press, 2001).

1. Introduction

The investigation of nonlinear optical processes in silicon-on-insulator (SOI) waveguides has reached a level of maturity that has allowed researchers to move beyond the proof-of-concept phase and into the practical application realm. In particular, the third-order nonlinear process of four-wave mixing (FWM) in silicon integrated waveguides has recently received particularly intense investigation due to the large third-order susceptibility ($\chi^{(3)}$) of silicon and a wavelength-tunable method of signal amplification, conversion, and regeneration is an extremely attractive capability in the silicon-on-insulator platform for integrated photonic circuits.

Initial experimental investigations into FWM in silicon waveguides [1,2] were successful due to the large pump powers and small modal areas of the waveguides used. The tight optical confinement of these waveguides ensured large optical intensities resulting in a measurable nonlinear response despite the lack of dispersion optimization. Subsequent investigations [3,4] demonstrated the ability to optimize not only the conversion efficiency but also the available bandwidth. This was accomplished by dispersion engineering the waveguide: tuning the waveguide modal dispersion to optimize phase matching at the wavelengths of interest. With the modal dispersion optimized, maximum conversion efficiencies of up to −9.6 dB and usable bandwidths greater than 150 nm have been demonstrated [3]. In addition to these optimizations, further enhancement of the FWM conversion efficiency has been demonstrated utilizing ring resonators [1,5,6], hybrid silicon-organic slot waveguide structures [7], and chalcogenide-based planar waveguides [8]. These promising proof-of-concept experiments have paved the way for the demonstration of practical applications of FWM in silicon. These applications include: wavelength conversion at 40 [9] and 160 GB/s [10], all optical signal regeneration [11], spectral phase conjugation [12], and waveform compression [13]. The utility of four-wave mixing in silicon waveguides has branched out beyond applications grounded in optical communications system and into a number of other areas. The realization that FWM could be utilized as an on-chip optical time lens [14] has led to a number of interesting new applications including temporal [15] and spectral magnification [16] and the demonstration of an ultrafast optical oscilloscope [17].

#126813 - $15.00 USD Received 12 Apr 2010; revised 22 Jun 2010; accepted 22 Jun 2010; published 7 Jul 2010

For the majority of applications of FWM in silicon waveguides, the length of the waveguide needed to achieve large conversion efficiency is typically on the order of several centimeters, occupying a large footprint on the photonic integrated circuit. Photonic crystal waveguides with slow-light modes, however, offer an approach to significantly increase the light-matter interaction with significantly (100 × or more) smaller footprints. The modes of a photonic crystal waveguide exhibit unique dispersion properties that have been demonstrated to exhibit large group indices [18–21]. Slow-light in two-dimensional, hexagonal photonic crystal single line-defect waveguides has been demonstrated to enhance a number of nonlinear phenomenon including Raman scattering [22,23], self-phase modulation [24–28], third-harmonic generation [29], in the presence of nonlinear absorption such as two-photon (TPA), three-photon, and free carrier absorption (FCA) [30].

In the specific case of slow-light enhancement of FWM in photonic crystal waveguides, the conversion efficiency has been theoretically suggested to be enhanced due to the increase in the effective length of the waveguide [31,32]. However, due to the large group velocity dispersion (GVD) of these waveguides in the slow-light regime, the conversion efficiency bandwidth is typically reduced. Four-wave mixing has been observed in silicon [33] and GaInP [34] photonic crystal waveguides previously. In addition, chalcogenide-based photonic crystal waveguide has observed conversion efficiencies 13 × higher than in silicon wire waveguides [35]. In this paper, we experimentally demonstrate the slow-light enhancement of the FWM conversion efficiency and corresponding shrinking of the conversion bandwidth due to the increase in GVD at large group index in W1 silicon photonic crystal waveguides.

2. Theory

In this experiment we examine the nonlinear optical process of partially degenerate four-wave mixing (FWM). In this process a pump wave (ω_{pump}) and a signal wave (ω_{signal}) couple power into an idler wave with an optical frequency determined by $\omega_{idler} = 2\omega_{pump} - \omega_{signal}$ via the third-order nonlinear susceptibility ($\chi^{(3)}$) of silicon. The efficiency of this exchange of energy is dependent on the level of coherence between all the frequencies involved (ω_{pump}, ω_{signal}, ω_{idler}) in order to maintain conservation of momentum. For optical waves confined to a guided mode structure, such as in a optical waveguide, the coherence is determined by the nonlinear and linear phase mismatch of the propagating modes. The lower the phase mismatch, the more efficiently the power transfers to ω_{idler}.

The goal of this work is to characterize the wavelength dependence of this conversion efficiency within a silicon W1 photonic crystal waveguide (PhCWG). The W1 waveguide is defined as a single line defect in a 2D photonic crystal created by a hexagonal array of holes in a silicon membrane. These waveguides exhibit very large anomalous dispersion owing to the optical mode being confined laterally by the photonic bandgap. Consequently, the group index of the waveguide increases monotonically with wavelength as it approaches the waveguide cut-off wavelength (λ_c), at which point the Bragg condition is satisfied allowing the forward and backward modes to couple and form a standing wave. This "slow-light" behavior allows for the enhancement of nonlinear optical phenomenon [36] due to the increased optical path length the larger group index introduces or more specifically: the light-matter interaction length is increased by the coherent Bragg reflections the optical mode experiences the closer the wavelength is to λ_c. The group index enhancement does not only limit itself to desired nonlinear effects therefore nonlinear absorption and scattering loses will be enhanced as well. However, it can be imagined that if the processes responsible for a desired nonlinear process and the unwanted process scale unequally, then the group index enhancement allows for achieving a desired nonlinear performance within a shorter length device. In addition to the enhancement of nonlinear absorption, the photonic crystal waveguides being investigated in this paper have the additional unwanted characteristic, in terms of FWM, of having large group velocity dispersion (GVD). The GVD of the waveguide

#126813 - $15.00 USD Received 12 Apr 2010; revised 22 Jun 2010; accepted 22 Jun 2010; published 7 Jul 2010

is the primary source of phase mismatch within the FWM process and its effect will be directly observed in this experiment. It is expected that GVD will be the limiting factor on the applicability of any observed enhancement as it will limit the maximum signal and pump wavelength separation that FWM can efficiently occur for.

In order to gauge the veracity of any observed FWM enhancement a simple numerical model will be employed. By extending previous work done in fibers [37], it has been shown [31] that for a photonic crystal waveguide of length *L*, the conversion efficiency is given by

$$\mathrm{G}_{idler} = \frac{\mathrm{P}_{idler}^{out}}{\mathrm{P}_{signal}^{in}} = \left(\frac{\gamma^* \overline{\mathrm{P}}_p}{g} \sinh\left(gL\right) \right)^2 e^{\alpha^*_{idler} L} \tag{1}$$

The efficiency is governed by an effective coupled pump power, $\overline{\mathrm{P}}_p = \mathrm{P}(0)\left(1 - e^{-\alpha^*_{pump}\mathrm{L}}\right) \Big/ \alpha^*_{pump}\mathrm{L}$, which accounts for the losses experienced by the pump wave during propagation through the waveguide. In order to account for the slow-light effect of the PhCWG, the nonlinear parameter (γ) and the waveguide linear propagation loss (α) have been substituted with group index dependent versions of themselves (γ^*, α^*). For the third-order nonlinear parameter the group index scaling is defined as [24] $\gamma^* = \gamma_0 \left(n_g / n_0\right)^2$, where $\gamma_0 = \omega_{pump} n_2 / cA_{eff}$. In the simulations presented within this paper the value of n_2 used was 4.5×10^{-16} m^2/W [38] and the effective mode area (A_{eff}) of the PhCWG mode, (averaged over a single unit volume of the waveguide [39]) was calculated to range from 0.24 μm^2 to 0.4 μm^2. The group index scaling of the propagation loss is defined as $\alpha^* = \alpha_0 \left(n_g / n_0\right)$, where the propagation loss scales linear with the group index. The justification for this choice of scaling will be addressed later in the paper.

In Eq. (1) the parametric gain, g, contains the phase dependent variables and is defined as

$$g = \sqrt{\left(\gamma^* \overline{P}_p\right)^2 - \left(\frac{\Delta k_L + \Delta k_{NL}}{2}\right)^2} \tag{2}$$

The linear phase mismatch between the interacting optical frequencies is $\Delta k_L = 2k_{pump} - k_{signal} - k_{idler}$ In order to examine the wavelength dependence of Δk_L it can be approximated using a Taylor expansion about the pump frequency given by

$$\Delta k_L \approx \left(\Delta w\right)^2 \beta_2\left(\lambda_{pump}\right) + \frac{1}{12}\left(\Delta w\right)^4 \beta_4\left(\lambda_{pump}\right) \tag{3}$$

where $\Delta\omega = \left|\omega_{pump} - \omega_{signal}\right|$ The dispersion dependent parameters, $\beta_2(\lambda)$ and $\beta_4(\lambda)$, are derived [40] from the numerically computed [41] dispersion relation of the guided mode of the PhCWG. In this work all wavelengths propagate in the fundamental quasi-TE guided mode of the PhCWG. The other phase term in Eq. (2), Δk_{NL}, is the nonlinear phase mismatch and is defined as

$$\Delta k_{NL} = 2\gamma^* \overline{P}_P \tag{4}$$

This simple model neglects nonlinear absorption effects such as two-photon and free-carrier absorption. However due to the relatively short length of our waveguide and the low coupled powers used it will be shown that these effects are minimal in these particular measurements and the model provides a confident representation of the basic trends of the underlying FWM.

#126813 - $15.00 USD Received 12 Apr 2010; revised 22 Jun 2010; accepted 22 Jun 2010; published 7 Jul 2010

3. Experiment

The W1 waveguide utilized in this experiment was fabricated using deep-UV photolithography on a silicon-on-insulator wafer with a silicon thickness of 250 nm and a buried oxide thickness of 1 μm. The lattice constant (a) for the hexagonal photonic crystal membrane was 440 nm and the radius of the fabricated holes was 0.36a (~158 nm). The total length of the PhCWG was 1000a (0.44 mm). The photonic crystal region was subjected to a hydrofluoric acid etch in order to remove the oxide beneath it, creating a suspended silicon membrane with air cladding above and below. The input and output of the PhCWG are butt coupled to channel waveguides. The input (output) channel waveguide tapers linearly from an initial width of $\sqrt{3}a$ ~0.76 μm at the PhCWG to a width of 4 μm (3.2 μm), over a length of 1.3 mm (0.8 mm). The transmission of TE polarized light through the device can be seen in seen in Fig. 1(a). The significant drop in transmission, which corresponds to the fundamental quasi-TE mode cut off wavelength (λ_c), can be seen to be near 1545.5 nm.

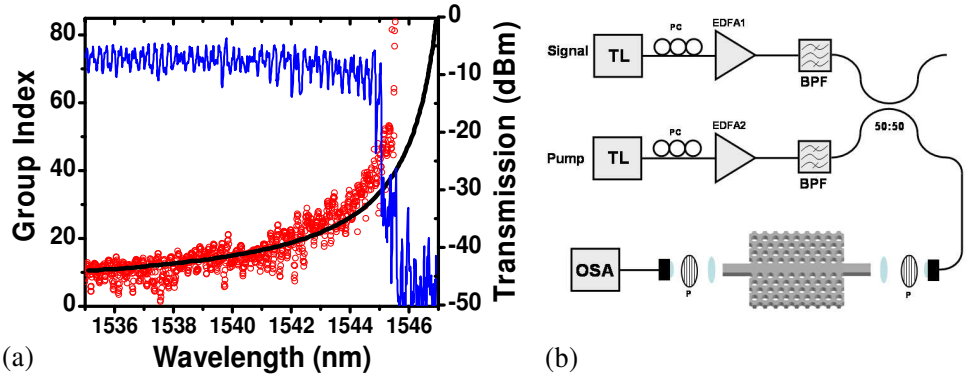

Fig. 1. (a) The optical transmission (blue line), measured group index (points), and fitted numerically calculated group index (black line). (b) Experimental setup for the measurement of partially degenerate four-wave mixing.

In order to determine the group index of the waveguide with respect to wavelength we employed the phase-delay method [42] in which the light from a tunable laser was modulated at a frequency of 5 GHz using a lithium niobate modulator and microwave synthesizer. The light was then transmitted through the waveguide, collected, and fed into a high-speed photoreceiver (bandwidth~15 GHz). The wavelength dependent time delay ($\tau(\lambda)$) between the transmitted waveform and the modulator driving signal was measured using a high speed sampling oscilloscope. The measured delay was used to compute the group index by from the relation $n_g(\lambda) = n_{wg} + \Delta n(\lambda) = n_{wg} + c\Delta\tau(\lambda)/L_{PhCWG}$, where $\Delta\tau(\lambda)$ is the measured time delay difference between the PhCWG and a channel waveguide of the same length with a known group index (n_{wg}, derived from numerical simulation). The group index is observed to increase rapidly as the wavelength approaches λ_c, confirmation that this is indeed the cutoff of the quasi-TE mode.

Degenerate four-wave mixing in the PhCWG was observed using the experimental setup in Fig. 1(b). Two tunable continuous-wave lasers were employed, one acting as a pump and the other as a signal probe, are both amplified using separate erbium doped fiber amplifiers and then subsequently optically filtered (3-dB bandwidth ~0.2 nm) of amplified spontaneous emission noise. The pump and signal were combined using a 50:50 fiber coupler and the combined wavelengths were coupled into the waveguide using an aspheric lens (NA = 0.6). The light exiting the waveguide was collimated back into fiber and analyzed using an optical spectrum analyzer (OSA) with 10 pm resolution. Taking into account filter loss, collimator

#126813 - $15.00 USD Received 12 Apr 2010; revised 22 Jun 2010; accepted 22 Jun 2010; published 7 Jul 2010

loss, and an 8.5 dB per facet coupling loss, the estimated coupled pump power and signal power was + 14 dBm and + 11 dBm respectively. All values reported for measured idler power are the powers measured at the OSA and therefore include the output coupling loss, as will be expanded upon when conversion efficiency is discussed .

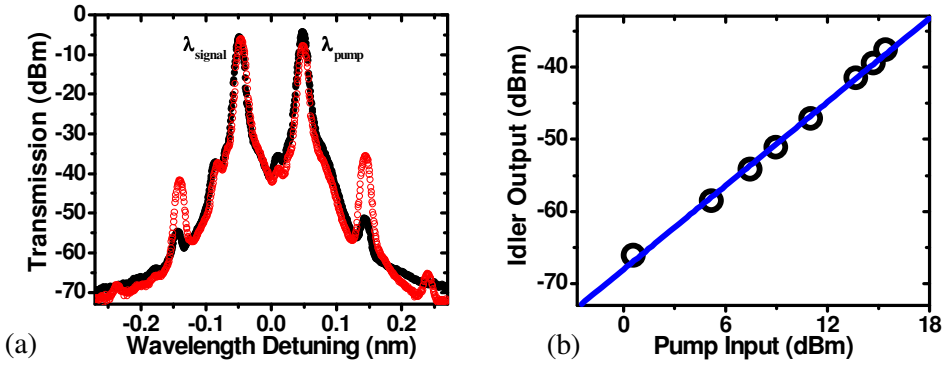

Fig. 2. (a) Optical spectrum of degenerate four-wave mixing in a W1 silicon photonic crystal waveguide. λ_{pump} = 1535.00 nm, $n_g \approx 10$ (black), λ_{pump} = 1545.75 nm, $n_g \approx 80$ (red) (b) Measured idler output for varying pump power (λ_{pump} = 1535.00 nm); measurement (points) linear fit, m = 1.92 (solid line).

Experimentally observed four-wave mixing in a silicon photonic crystal waveguide for two different wavelengths (λ_{pump} = 1535.00 nm and λ_{pump} = 1545.75 nm) can be seen in Fig. 2(a). In both measured spectra the difference between the pump and signal is ~0.1 nm, the pump being defined as the high wavelength laser (the peak at + 0.05 nm). As can be seen from this data, the generated idler power for the case of the high group index (1545.75 nm, n_g ~80) is greater than that of lower group index (1535.00 nm, n_g ~10). As further evidence of increased FWM conversion efficiency at the higher group index wavelength is that the higher order idler (small peaks at ± 0.24 nm), which are generated from cascaded parametric mixing of the signal and pump with their fundamental idler. Also of note in Fig. 2(a) is the attenuation of the transmitted pump wavelength at slow-light which is due in part to it experiencing a higher group index enhanced propagation loss and also due to the strong Fabry-Perot oscillations at these wavelengths. In order to gauge whether any nonlinear absorption could be observed, the pump power dependence of the idler for λ_{pump} = 1535.00 nm was measured for varying pump input powers and plotted in Fig. 2(b). The resulting linear fit gives a slope of 1.92, close to the expected 2 the quadratic dependence would display on such a log-log plot.

In order to investigate the wavelength dependence of the four wave mixing process within the waveguide, the generated idler power at $2\omega_{pump}$- ω_{signal} was measured for signal wavelengths −5 nm to + 5 nm detuned from the pump wavelength in 0.1 nm steps. This was done for pump wavelengths from 1535 to 1545.5 nm in 0.5 nm steps. The resulting two-dimensional map of measured idler powers can be seen in Fig. 3(a). To corroborate the measured results the model outlined was used with the numerically computed dispersion; the result of which can be seen in Fig. 3(b). Since the value being plotted here is the power measured at the OSA, the value actually measured is ηP_{idler}^{out}, where η is the output coupling loss. In the model, in order to compare with measurements, we numerically computed $\eta P_{signal}^{in} G_{idler}$ and in order to be consistent, the model is computed with the same wavelength steps as the experimental data ($\Delta\lambda_{signal}$ = 0.1 nm, $\Delta\lambda_{pump}$ = 0.5 nm). Slices from the 2D figures that directly compare the measured results and the numerical model for λ_{pump} = 1535.0 nm and λ_{pump} = 1545.5 nm are plotted in Fig. 3(c). The maximum measured idler power for each pump wavelength is plotted in Fig. 3(d).

#126813 - $15.00 USD Received 12 Apr 2010; revised 22 Jun 2010; accepted 22 Jun 2010; published 7 Jul 2010

The free parameters used to fit the numerical model with the experimental data were an absolute wavelength shift of the numerically simulated group index data from which $\beta_2(\lambda)$ and $\beta_4(\lambda)$ are derived from, $n_g^{\text{model}}(\lambda) = n_g^{\text{sim}}(\lambda + \lambda_0\Delta)$, where λ_0 = 1535nm, and the value of the minimum linear propagation loss, α_0. The group index shift was determined by finding the value of Δ that produced the best match to experimental results for the λ_{pump} = 1535 nm data plotted in Fig. 3(c). The best fit was achieved for $\Delta = -2.6\%$, equivalent to a shift of ~40 nm in the absolute wavelength of the numerically simulated dispersion. This blue shift of the numerically calculated dispersion, when compared to experimental results, can be attributed to the thinning of the silicon slab thickness during the wet oxide etch [43]. A 2.6% blue-shift in wavelength corresponds to a reduction in the silicon slab thickness by approximately 24 nm (9.6% of the slab thickness). It is worth noting that this method of utilizing the idler power dependence on signal detuning at a wavelength far from the λ_c has advantages over conventional dispersion fitting methods. The method allows for direct examination of dispersion difference of the PhCWG and the simulated dispersion and is not dependant on exactly where λ_c occurs [44], which can be impossible for long waveguides where λ_c and the minimum transmission might not coincide or for waveguides with large disorder which can cause a broadening of λ_c. In addition, the method appears immune to the broadening of the phase-delay response (See Fig. 1(a)) of the waveguide which is due to the etalon effects of the waveguide facets. The minimum propagation loss which gave the best reproduction of the experiment was 10 dB/cm. This resulting value of α_0 is lower than what we have measured using the cut-back method for similarly fabricated waveguides (~20 dB/cm), but this value of α_0 is not out of the realm of possibility, devices fabricated in a similar manner (deep-UV photolithography) have shown losses as low 14 dB/cm [45].

The calculated wavelength dependence of the generated idler power matches closely with that of the measured results and the idler power is observed to increase by over 12 dB when the pump wavelength is translated to a wavelength in the vicinity of λ_c, while at the same time the bandwidth over which a measurable idler signal is observed decreases appreciably. This is mostly in good agreement with previously reported theoretical analysis [31], except for a noticeable asymmetry of the generated idler power about the pump wavelength in the experimental results. This asymmetry is attributed to the fact that for signal wavelengths blue shifted from the pump wavelength (signal detuning < 0 nm) generate idlers at wavelengths closer to λ_c or even beyond it, leading to larger propagation losses for these wavelengths. This becomes more apparent as the pump wavelength approaches λ_c, as can be seen in the plot for λ_{pump} = 1545.5 nm in Fig. 3(c) where the measured idler power is seen to drop by 14 dBm from –0.1 nm to –0.2 nm. This asymmetry is captured in the model by ensuring the proper group index is used to scale the loss at the wavelength that it is being applied.

#126813 - $15.00 USD Received 12 Apr 2010; revised 22 Jun 2010; accepted 22 Jun 2010; published 7 Jul 2010

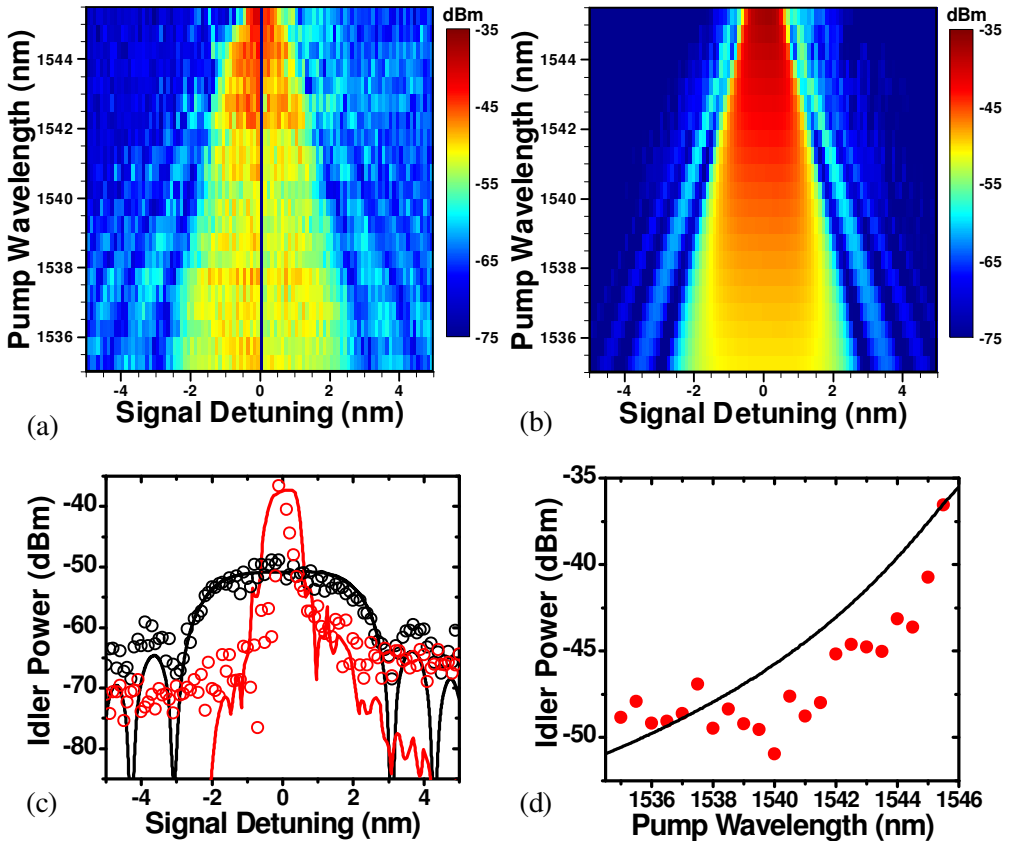

Fig. 3. (a) Measured idler power wavelength dependence ($\Delta\lambda_{pump}$ = 0.5 nm, $\Delta\lambda_{signal}$ = 0.1 nm) (b) Simulated idler power wavelength dependence (c) Idler power dependence for λ_{pump} = 1535.0 nm (black) and λ_{pump} = 1545.5 nm (red). (d) Maximum measured idler power versus pump wavelength; measurement (points), calculation (solid line).

Our analysis of the experimental data and modeling ignores the contribution to the measured idler that the input and output tapered waveguides contribute, making the assumption that the measured idler power is primarily generated in the PhCWG. This may seem like a strange assumption considering the PhCWG makes up only 20% of the total length of the device however the measured data shows that this assumption is valid by displaying two distinct features as the pump wavelength approaches λ_c: a decreasing bandwidth over which an idler signal is measured and an increase in idler power while incident pump and signal powers are constant. The first observation, the decrease in bandwidth, is a direct result of the fact that the GVD of the PhCWG is at least two orders of magnitude larger than what would be found in waveguides with widths experienced in the tapered waveguides. The $\beta_2(\lambda)$ and $\beta_4(\lambda)$ for the PhCWG used in this experiment is plotted in Fig. 4(a), along with the $\beta_2(\lambda)$ of conventional waveguides, calculated using the plane wave expansion method [41] incorporating the material dispersion of silicon, with widths within the range of the input/output tapered waveguides for comparison. Consequently, if the idler was being primarily generated inside the input/output tapered waveguides it would show little variation in idler output power for ± 5 nm signal detunings. A 3.5 mm long silicon waveguide has been shown [1] to have a flat response for over ± 20 nm pump-signal detuning. As our total device length is only 2.5 mm, it would be expected to have an even better detuning performance, yet it only has a maximum flat response over ± 2.5 nm, significantly

#126813 - $15.00 USD Received 12 Apr 2010; revised 22 Jun 2010; accepted 22 Jun 2010; published 7 Jul 2010

smaller and an indication that the idler is being generated in the PhCWG, where there is a much higher GVD. In addition to this bandwidth reduction, the decaying oscillatory peaks of Eq. (1) are resolved in the experimental data of Fig. 3(a) and 3(c). If there was a strong detuning independent (over the ± 5 nm detuning examined here) idler being generated in the channel waveguides it would be expected these oscillations would be washed out and unable to be resolved.

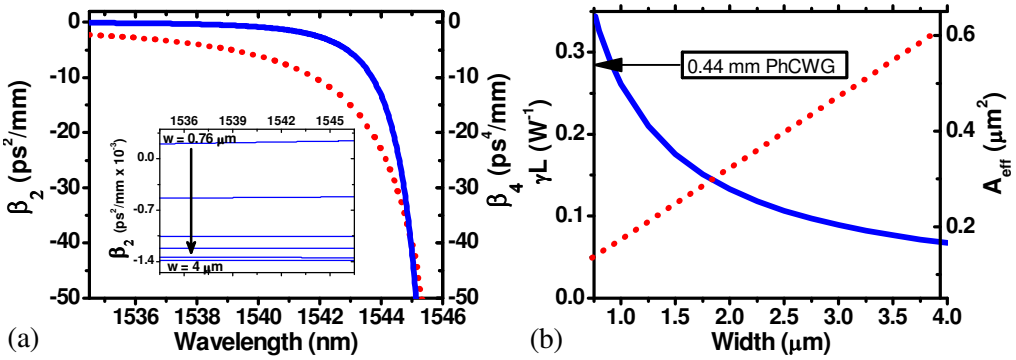

Fig. 4. (a) β_2 (solid line) and β_4 (dotted line) for the photonic crystal waveguide used in this experiment (inset) β_2 for conventional silicon waveguides for various widths (0.76 μm, 1.0 μm, 1.5 μm, 2.0 μm, 3.0 μm, and 4.0 μm) (b) Calculated γL value (solid line) and the A_{eff}(dotted line) versus waveguide width. Arrow indicates the expected minimum (λ_{pump} = 1535) value of $\gamma^* L$ for a 0.44 mm PhCWG (channel waveguide length = 2.1 mm, height = 0.25 μm)

In addition to the observed bandwidth contraction, the measured idler power is observed to increase as the pump wavelength approaches λ_c for fixed pump and signal powers, a telling sign of group index enhancement of the nonlinear parameter. Especially when one considers that the transmission of the waveguide experiences a 5dB drop in transmission between these two wavelengths. In order to justify that the 0.44 mm long PhCWG by itself is responsible we compare it to a theoretical 2.1 mm (the total length of the device minus the length of the PhCWG) long channel waveguide by plotting the $\gamma L = \omega_{pump} n_2 / c A_{eff}$ parameter value for a for widths within the range of the taper used in our device, as well as the minimum $\gamma^* L$ value expected from the 0.44 mm PhCWG. The 0.44 mm long PhCWG shows a larger nonlinear response than the majority of the 2.1 mm long waveguides with widths experienced in the tapered. It is only overtaken by the conventional waveguides when their effective area becomes small enough to compensate for the group index enhancement in the PhCWG. However, the effective area of the conventional waveguide remains relatively constant over the wavelengths investigated here while the PhCWG sees an eight fold increase in group index. Therefore the pump wavelength dependence of the channel waveguides nonlinear parameter can be expected to be flat over the wavelengths examined, while the PhCWGs nonlinear parameter is expected to scale with the square of the group index. Additionally, the actual input/output channel waveguides used in the experiment have a linear taper in width going from the minimum of 0.76 μm to the maximum of 4 μm, therefore a more realistic value we should compare to would be the average γL value of the widths, which is ~14 and is half the minimum value expected from the PhCWG. Of course this simple comparison ignores the losses incurred from the PhCWG that occurs between the two channel waveguides in the actual experimental device, which if considered would further show that the idler power measured in the experiment is generated primarily within the PhCWG.

#126813 - $15.00 USD Received 12 Apr 2010; revised 22 Jun 2010; accepted 22 Jun 2010; published 7 Jul 2010

4. Results

In order to quantify the FWM process in the PhCWG, the measured idler powers should be normalized with respect to the coupled signal power in order to gauge the conversion efficiency. The conversion efficiency is derived experimentally by taking the ratio of the measured output idler power and measured output signal power $\left(\eta P_{idler}^{out} / \eta P_{signal}^{out}\right)$ in order to cancel any uncertainty in the coupling efficiency. It has recently been demonstrated [46] that using this definition can inadvertently overestimate conversion efficiency in silicon channel waveguides due to loss experienced by the signal within the waveguide, either through conventional linear propagation loss or by nonlinear loss due to two-photon and free-carrier absorption. In order to avoid this, the conversion efficiency can be defined as $P_{idler}^{out} / P_{signal}^{in}$. Using this definition the maximum conversion efficiency of our waveguide for this pump power is derived from the maximum measured idler power $\max\left(\eta P_{idler}^{out}\right)$ = −35.6 dBm, (see Fig. 3(d)) and knowing that P_{signal}^{in} is + 11.5 dBm and that the coupling loss is estimated to be 8.5 dB a maximum measured conversion efficiency of −38.8 dB is found. We can conclude that this value is the lower bound estimate of the maximum conversion efficiency of our waveguide for this coupled pump power. The assumption made with this definition is that the coupling to the waveguide of both the pump and signal is wavelength independent, which is valid for channel waveguides for the bandwidths considered here but not for a photonic crystal waveguide which exhibits increased coupling losses as the group index of the PhCWG mode increases.

With the lower bound conversion efficiency of the experiment stated, we will now present the results for the conventional definition ($\eta P_{idler}^{out} / \eta P_{signal}^{out}$) (where ηP_{signal}^{out} is measured with the pump off), in order to make an attempt at correcting for this group index dependent coupling loss. In order for this definition to be valid the conversion efficiencies will be derived from the maximum idler power generated by a signal detuned ± 0.1 nm from the pump wavelength in order to minimize any difference in the group index dependent coupling loss experienced by the idler and signal. The pump wavelength dependence of this conversion efficiency is plotted in Fig. 5(a). The maximum measured conversion efficiency, using the ($\eta P_{idler}^{out} / \eta P_{signal}^{out}$) definition, is −35.7 dB; a difference of ~3 dB compared with the lower bound. This difference stems from the fact that the assumption that the idler and signal are experiencing equivalent coupling and propagation losses begins to break down at large group indices. For these pump wavelengths the maximum generated idler occurs when the signal is red shifted from the pump and consequently experiencing a higher group index and higher losses. This artificial increase in conversion efficiency could be mitigated by reducing the wavelength separation between the pump and signal however we are limited by our filter bandwidths and OSA resolution. In order to explicitly display that the increase in the group index is responsible for the enhancement of the conversion efficiency it is plotted versus group index in Fig. 5(b). In plotting the experimentally measured conversion efficiency, the measured group index is used (red points in Fig. 1(a)) and the wavelength shifted numerically computed group index is used to plot the model conversion efficiency.

The numerical model appears to underestimate the maximum conversion efficiency by 5 dB, which would appear counterintuitive since the simulation does not take into account the decrease in the amount of pump power coupling into the waveguide as the group index increases. It would be expected that because of this fact the numerical model should show higher maximum conversion efficiencies than the experiment. This discrepancy can be attributed to the fact that this simple numerical model does not account for the effect the finite size of the PhCWG has on its transmission, which is responsible for the increasing strength and frequency of the Fabry-Perot oscillations as the cutoff wavelength is approached [18]. A

#126813 - $15.00 USD Received 12 Apr 2010; revised 22 Jun 2010; accepted 22 Jun 2010; published 7 Jul 2010

decrease in the pump and signal wavelength step sizes ($\Delta\lambda_{signal}$, $\Delta\lambda_{pump}$) would be expected to reveal the measured data points oscillating about a trend more in line with what is expected. The strength of the Fabry-Perot oscillations can be reduced through proper impedance matching of the channel waveguide and the PhCWG [48]. The high resolution data would also make it possible to accurately probe the dispersion and observe the wavelength/group index at which point disorder can no longer be considered perturbative [49].

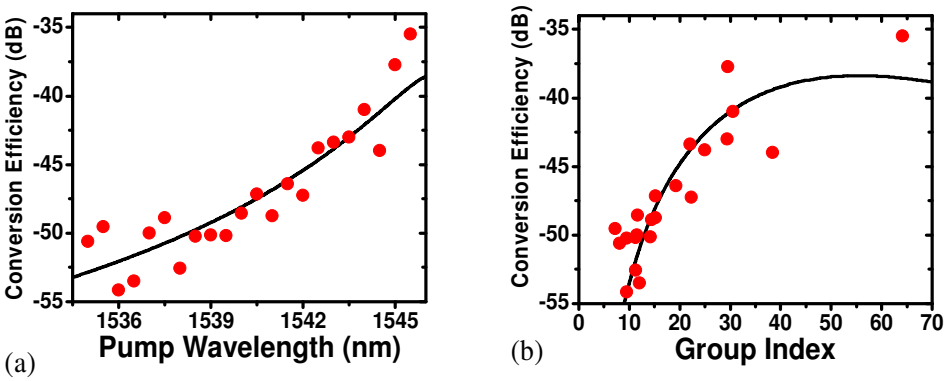

Fig. 5. (a) Four-wave mixing conversion efficiency dependence on pump wavelength ($|\lambda_{signal}-\lambda_{pump}| = 0.1$nm). (b) Conversion Efficiency dependence on n_g at λ_{pump}; measurement (points), calculation (solid line).

As was discussed previously, the large dispersion of the PhCWG is responsible for the reduction in the bandwidth over which an appreciable idler power is measured as the pump wavelength gets closer to λ_c. The increasing values of $\beta_2(\lambda)$ and $\beta_4(\lambda)$ (See Fig. 4(a)) cause a larger phase mismatch between the interacting wavelengths within the propagation length of the PhCWG, resulting in the efficiency of conversion falling off more quickly with respect to pump and signal detuning. This phenomenon can be directly observed in the experimental data in Fig. 3(a) by observing the shrinking signal detuning bandwidth over which a measurable idler power is observed as the pump wavelength moves towards λ_c, giving the plot a distinctive triangular appearance. This limitation of the W1 waveguide has been reported previously [31] and can be mitigated by the introduction of regions of low-GVD into the waveguide dispersion by structural optimization [50,25].

To characterize the decrease in the FWM bandwidth as the pump is moved closer to λ_c the bandwidth of the measured conversion efficiency is plotted in Fig. 6(a). Due to the strong Fabry-Perot oscillations and limited resolution of the experimental data a conventional −3dB bandwidth could not be accurately gauged so we define the bandwidth as the total detuning range over which the conversion efficiency is within −10 dB of the maximum value for each pump wavelength. The same definition is applied to the simulated data to derive the bandwidth from the model. The measured results agree well with the model except for the last two measured pump wavelengths. This can be attributed to the imperfect match between the measured group index and the shifted numerically derived group index used for the model (illustrated in Fig. 1(a)) at these wavelengths. However, when the measured bandwidth is plotted with respect to group index, as it is in Fig. 6(b), this discrepancy is removed. The remaining deviations between experiment and model here are attributable to the finite signal wavelength step (0.1 nm) and the Fabry-Perot induced uncertainty in both the group index when using the phase shift method [51] and transmission when determining the −10 dB wavelengths.

#126813 - $15.00 USD Received 12 Apr 2010; revised 22 Jun 2010; accepted 22 Jun 2010; published 7 Jul 2010

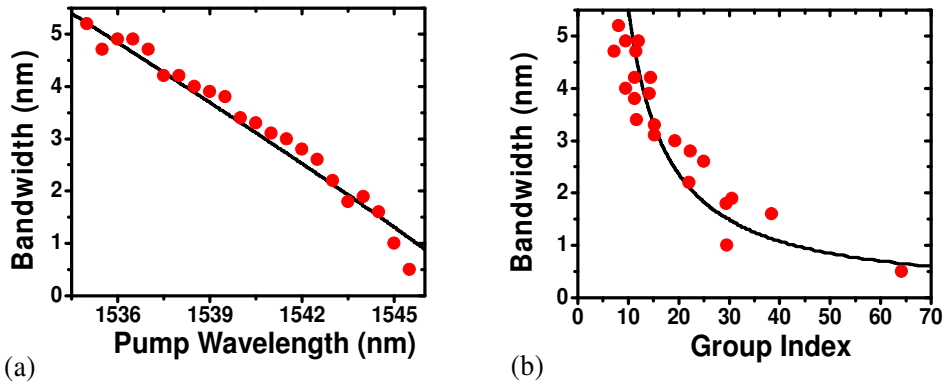

Fig. 6. The −10-dB bandwidth dependence on (a) λ_{pump} and (b) n_g (at λ_{pump}); measurement (points), calculation (solid line).

It was stated previously that the model employed in this work uses a linear group index (n_g) scaling of the linear propagation loss: $\alpha^* = \alpha_0 \left(n_g / n_0 \right)$, where α_0, the minimum propagation loss, was 10 dB/cm. A linear scaling of loss with respect to group index was chosen because it was found to give the best fit to the experimental data. This fact is illustrated in Fig. 7 where the data presented in Fig. 5(b) is shown with the conversion efficiency of the model for different propagation loss n_g scaling factors with all other variables being equal. A number of recent experiments and theoretical investigations on the exact scaling of loss, both scattering loss due to fabrication disorder and loss caused by coupling to the backward propagating mode, with respect to group index in photonic crystal waveguides has provided a number of differing opinions on the subject [49,52–55], with several reports concluding that the fabrication disorder-induced loss in photonic crystal waveguides, like that of regular channel waveguides [56], scaling linearly with group index and that the loss from scattering of the forward propagating mode into the backward propagating mode scaling quadratically with group index. However, fabrication disorder can cause coherent scattering within and between unit cells of the waveguide along the direction of propagation [57]. In addition, there is a modification of the propagating Bloch mode shape with respect to frequency which has the effect of increasing the disorder sampling. These two factors have been used to suggest that the Beer-Lambert law and the simplistic view of relating group index scaling of loss fail for large group indices [58]. In regards to this experiment, since the majority of the data collected was in the n_g less than 40 regime, the dominant scaling of propagation loss observed in this experiment was linear.

One other possible source of experimental uncertainty with regard to the group index at λ_{pump} comes from the thermal shift of λ_c due to the presence of the pump beam. The thermal heating of the sample caused by the pump beam would cause a red-shift in the cutoff wavelength in contrast to the data presented in Fig. 1(a) which was collected at low optical powers. It is understandable that the waveguide would be more susceptible to the thermo-optic shifting of λ_c the larger the group index of the pump beam is, owing to the group index enhancement of optical intensity. However, due to the agreement between the calculated and measured bandwidth (see Fig. 6), which is directly dependant on the value of β_2 [59], we are confident that thermal shift of the group index value is minimal.

#126813 - $15.00 USD Received 12 Apr 2010; revised 22 Jun 2010; accepted 22 Jun 2010; published 7 Jul 2010

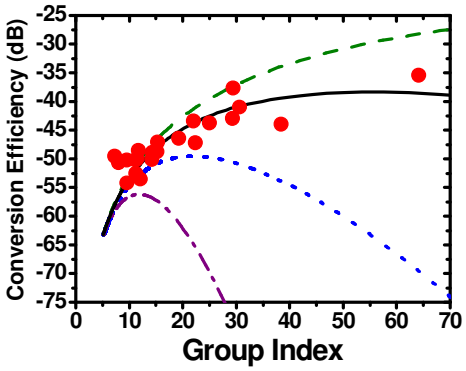

Fig. 7. Conversion Efficiency dependence on n_g at λ_{pump} for different propagation loss n_g scaling factors: $\alpha^* = \alpha_0 \left(n_g / n_0 \right)^{\delta}$; $\delta = \sqrt{2}/2$ (dash), $\delta = 1$ (solid), $\delta = \sqrt{2}$ (dot), $\delta = 2$ (dash-dot), measurement (solid points).

5. Conclusion

We have experimentally investigated the group index enhancement of four-wave mixing in a W1 silicon photonic crystal waveguides. A 0.44 mm long waveguide exhibited a maximum conversion efficiency of −36 dB using a coupled pump power of 14 dBm. Over the wavelengths examined a group index enhancement of the third-order nonlinearity resulting in the conversion efficiency was to increase by over 12 dB from a $\Delta n_g \approx 55$. A corresponding decrease in the conversion efficiency bandwidth, from 5 nm to 0.5 nm, was also observed, which would severely limit the utility of the device in regard to most known applications of FWM in conventional silicon waveguide. Both of these experimental observations match well with a simple numerical model of four-wave mixing in photonic crystal waveguides which accounts for group index scaling of the propagation loss and nonlinear. The results presented here reinforce the slow-light nonlinear enhancement possible within silicon photonic crystal waveguides.

Acknowledgments

The authors acknowledge discussions with C. A. Husko, M.-C. Wu, and N. C. Panoiu. This work is supported by NSF (ECCS-0622069 and ECCS-0747787).

#126813 - $15.00 USD Received 12 Apr 2010; revised 22 Jun 2010; accepted 22 Jun 2010; published 7 Jul 2010